Granular superconductivity and charge/orbital order in $YBa_2Cu_3O_7$/manganite trilayers

J. Khmaladze,[1] S. Sarkar,[1] M. Soulier,[1] F. Lyzwa,[1] R. de Andres Prada,[1] E. Perret,[1,2] B. P. P. Mallett,[3] M. Minola,[4] B. Keimer,[4] and C. Bernhard[1]

[1]*Department of Physics and Fribourg Center for Nanomaterials, University of Fribourg, Chemin du Musée 3, 1700 Fribourg, Switzerland*
[2]*Laboratory for Advanced Fibers, Empa, Swiss Federal Laboratories for Materials Science and Technology, Lerchenfeldstrasse 5, 9014 St. Gallen, Switzerland*
[3]*The MacDiarmid Institute and the Dodd Walls Centre for Photonic and Quantum Technologies, Photon Factory, University of Auckland, 38 Princes St., Auckland, New Zealand*
[4]*Max-Planck-Institut für Festkörperforschung, Heisenbergstrasse 1, 70569 Stuttgart, Germany*

(Received 26 April 2019; revised manuscript received 17 June 2019; published 1 August 2019)

We studied how the electronic, superconducting, and magnetic properties of $YBa_2Cu_3O_7$/$Nd_{1-x}(Ca_{1-y}Sr_y)_xMnO_3$ multilayers depend on the tolerance factor and the hole doping of the manganite. In particular, we investigated the granular superconducting state and the related magnetic-field-driven insulator-to-superconductor transition that was previously discovered in corresponding multilayers with $Pr_{0.5}La_{0.2}Ca_{0.3}MnO_3$ [B. P. P. Mallett *et al.*, Phys. Rev. B **94**, 180503(R) (2016)]. We found that this granular superconducting state occurs only when the manganite layer is in a charge/orbital ordered and CE-type antiferromagnetic state (Mn-CO/OO). The coupling mechanism underlying this intriguing proximity effect seems to involve the domain boundaries of the Mn-CO/OO and/or the charge disordered regions of the manganite layer that become more numerous as the hole doping is reduced below $x = 0.5$.

DOI: 10.1103/PhysRevMaterials.3.084801

I. INTRODUCTION

High-T_c superconductivity in the cuprates [1] and the colossal magnetoresistance (CMR) effect of the perovskite manganites [2] are prominent examples of the exceptional electronic properties of the complex oxides with strongly correlated electrons. These oxides tend to have strongly coupled charge, orbital, spin, and lattice degrees of freedom that can result in a complex behavior with multiple, nearly degenerate orders that interact and compete with each other [3–5]. The phase diagram of the perovskite manganites $A_{1-x}(Ca_{1-y}Sr_y)_xMnO_3$ (A = La or a trivalent rare earth) contains several insulating and metallic phases with different orbital and magnetic orders as a function of the hole doping (Mn^{3+}/Mn^{4+} ratio) and the tolerance factor, $t = (r_A + r_O)/\sqrt{2}(r_{Mn} + r_O)$, where r_A, r_O, and r_{Mn} are the radii of the A-site cation, oxygen, and manganese, respectively [6,7]. The tolerance factor determines the Mn-O-Mn bond angle and thus the bandwidth and the kinetic energy of the itinerant charge carriers. Likewise, for the cuprates there is evidence that charge and/or spin density wave orders (or even more exotic so-called hidden orders) compete with high-T_c superconductivity or may even form a so-called intertwined state [8]. Prominent examples are the stripe phase of La-based cuprates [9] and the ubiquitous incommensurate charge-density waves observed in other cuprate families [10].

An additional platform for testing and controlling the competition between different orders has emerged from the progress in growing heterostructures based on thin active layers of these complex oxides with well-defined and atomically sharp interfaces [4,11–13]. A well-studied example are multilayers comprised of the cuprate high-T_c superconductor YBa_2CuO_7 (YBCO), with a bulk critical temperature $T_c \approx$ 90 K, and the CMR manganites $La_{2/3}Ca_{1/3}MnO_3$ (LCMO) and $La_{2/3}Sr_{1/3}MnO_3$ (LSMO) with bulk ferromagnetic transition temperatures $T_{Curie} \approx 270$ and 330 K, respectively, and saturation moment of about 3.7 μ_B per Mn ion [14–33]. The focus of the initial work on these multilayers was on the competition between the antagonistic superconducting and ferromagnetic orders and was motivated by the progress with superconductor/ferromagnet heterostructures based on conventional superconductors, like Nb, Pb, or Al, and conventional ferromagnets, like Gd, Fe, Co, Ni, or permalloy. In these systems, a range of exotic orders have been realized, including a spin-triplet superconducting order parameter that generates spin-polarized supercurrents that may be used in future superspintronic quantum devices [34,35]. In comparison, the research on the cuprate/manganite multilayers is less advanced and still aimed at developing a better understanding of the basic phenomena that occur at these interfaces. Crucially, an electron transfer across the interface, from the manganite to the YBCO layer, and an orbital reconstruction of the interfacial Cu ions have been identified [24,25,33]. The latter originates from a strong covalent bonding between the interfacial Cu and Mn ions via the apical oxygen. This leads to a redistribution of the holes on the Cu ions from the $d_{x^2-y^2}$ orbital (where they reside in bulk cuprates) toward the $d_{z^2-r^2}$ orbital. Along with this orbital reconstruction comes an induced ferromagnetic moment of the interfacial Cu ions that aligns antiparallel to the Mn moment [24,33]. Nevertheless, the superconducting response of these YBCO/LCMO multilayers is only moderately affected by the exchange coupling to the ferromagnetic Mn moments and the induced Cu moments, and a reasonably sharp SC transition with $T_c > 60$ K can be realized, as long as the YBCO layer consists of at least

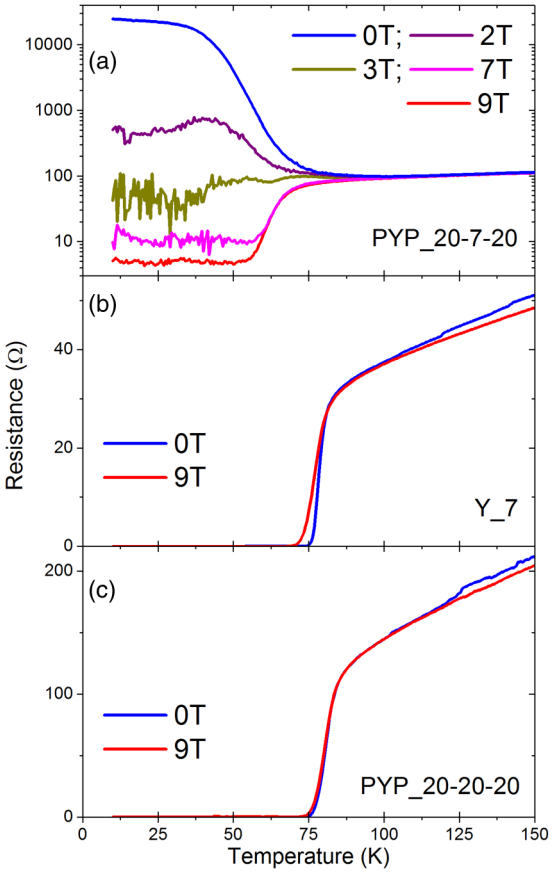

FIG. 1. Magnetoresistance vs temperature curves of thin films and multilayers from $Pr_{0.5}La_{0.2}Ca_{0.3}MnO_3$ (PLCMO) and $YBa_2Cu_3O_7$ (YBCO). (a) For a PLCMO(20 nm)/YBCO(7 nm)/PLCMO(20 nm) trilayer that was already discussed in Ref. [36], (b) for a YBCO(7 nm) single layer, and (c) for a PLCMO(20 nm)/YBCO(20 nm)/PLCMO(20 nm) trilayer.

four monolayers [20,28,31]. This is the minimal thickness for which the central CuO_2 layers are still sufficiently hole-doped for superconductivity to occur. Note that in addition to the interfacial electron transfer from LCMO to YBCO, the YBCO monolayers at the top and bottom interfaces are both lacking the CuO chain layer and thus their charge reservoir [18,25,28].

It is thus rather surprising that a severe suppression of the superconducting response was observed in YBCO/$Pr_{0.5}La_{0.2}Ca_{0.3}MnO_3$ (PLCMO) multilayers for which the YBCO layer consists of six monolayers ($d_{YBCO} \approx 7$ nm) [36]. Instead of a superconducting transition, they exhibit an insulator-like upturn of the dc resistivity toward low temperature. An example of this behavior is shown in Fig. 1(a) (blue line). Here the manganite layer is not a ferromagnetic half-metal but an insulator with a CE-type antiferromagnetic order and a combined charge and orbital ordered (CO/OO) state with wave vectors $Q_{OO} = (1/4, 1/4, 0)$ and $Q_{CO} = (1/2, 0, 0)$ or $(0, 1/2, 0)$ (expressed in reciprocal lattice units in pseudocubic notation) that develops below 220–240 K [6,7,36]. While there is evidence that the oxygen ions also play an important role in this CO/OO [37,38], for simplicity in the following we refer to it as Mn-CO/OO.

The insulating and Mn-CO/OO state of PLCMO, as compared to the half-metallic state of $La_{2/3}Ca_{1/3}MnO_3$ and $La_{2/3}Sr_{1/3}MnO_3$, is the result of a reduction of the tolerance factor, since La^{3+} ions with $r_{La} = 1.34$ Å are replaced by Pr^{3+} with r_{La}=1.29 Å, thereby leading to a larger tilting of the Mn-O-Mn bonds. This reduces the bandwidth and thus the potential gain in kinetic energy of the itinerant ferromagnetic state mediated by the double-exchange interaction [6,7]. Instead, the ground state is governed by the competing Jahn-Teller distortions of the oxygen octahedra that localize the charge carriers and thus favor an antiferromagnetic superexchange. In the Mn-CO/OO state, these Jahn-Teller distortions become cooperative and develop a coherent superstructure [6,7].

Notably, the highly resistive state of these YBCO/PLCMO multilayers can be suppressed with a large magnetic field, which also restores a regular superconducting response with a reasonably sharp resistive transition around $T_c \approx 75$ K, as shown in Fig. 1(a) (red line). Such a magnetic-field-induced insulator-to-superconductor transition (IST) is a highly unusual phenomenon since magnetic fields normally weaken and suppress superconductivity, rather than enhancing it [39,40]. Only a few exceptions are known, such as the so-called Jaccarino-Peter effect [41], which arises in the Chevrel phase $Eu_xSn_{1+x}Mo_6S_8$ [42], and the organic λ-$(BETS)_2FeCl_4$ [43], where the magnetic field compensates for a negative exchange field from magnetic ions that would otherwise destroy superconductivity by strong pair breaking. Furthermore, a reentrance of superconductivity (at very low temperature) was reported for Zn nanowires for which the dissipation of quasiparticles generated by a magnetic field counteracts quantum fluctuations that are detrimental to superconductivity [44,45].

As outlined in the following, the magnetic-field-induced IST in the YBCO/PLCMO multilayers appears to be of a different kind. The insulator-like response at low magnetic field cannot be explained in terms of a superconducting pair breaking effect that should restore the metallic normal-state properties (possibly with an enhanced scattering rate). Instead, there exists evidence for a granular superconducting state with grains that are strongly superconducting and boundaries at which the macroscopic coherence of the superconducting wave function is broken. A terahertz spectroscopy study in zero magnetic field has indeed revealed a strong plasmonic mode at nonzero frequency that develops below 80 K and arises from a strongly confined superconducting condensate [36].

Another characteristic feature of a granular superconducting state is the comparable temperature range in which both the resistive upturn in zero magnetic field and the downturn due to the superconducting transition at 9 T occur. The insulator-like state at low magnetic field thus seems to arise from a Coulomb-blocking that occurs when the repulsion between the Cooper pairs on the individual superconducting grains outweighs the Josephson coupling between the grains [39,40]. Note that the Heisenberg uncertainty principle relates the phase fluctuations of the SC wave function to the uncertainty of the number of Cooper pairs, i.e., the phase coherence is linked to the charge fluctuations.

For thin films of conventional superconductors, like Pb, such a granular superconducting state can be achieved if the grain boundaries are oxidized and thus become insulating

[39,40]. An IST is induced here as the thickness of the granular films is reduced. Likewise, such a highly resistive state due to localized Cooper pairs has been observed in nanofabricated Josephson- junctions networks [39,40,46].

For the present YBCO/PLCMO multilayers, this raises the question about the origin of this granular superconducting state and especially of the domain boundaries, which break the superconducting phase coherence in zero magnetic field, but not in very large magnetic fields. This granularity of the superconducting state of the YBCO layer can hardly be explained in terms of structural defects and impurities that should also deteriorate the normal state transport (contrary to the observed metallic response) and should not be suppressed by a magnetic field. It seems more likely that the granular superconductivity in the YBCO layer is induced by the interfacial coupling with a domain state of the Mn-CO/OO and the related complex magnetic order within the PLCMO layers. The latter may serve as a template for the granular superconducting state in the YBCO layer. It is indeed well-established that the Mn-COO order and the concomitant Jahn-Teller distortions in these manganites are weakened and eventually get suppressed by a large magnetic field, which strengthens the double-exchange mechanism and thus eventually restore an itinerant ferromagnetic state [6,7]. Yet, the exact nature of this domain state in the manganite layers, the mechanism of the interfacial coupling with the YBCO layer, and the properties of the induced domain state in the YBCO layer remain to be understood.

Here we address this issue by studying how the transport and magnetic properties of these YBCO/manganite multilayers evolve as a function of the tolerance factor, t (bandwidth), and/or the hole doping, x (band filling), which allows us to vary the strength and the correlation range of the Mn-CO/OO and of the related Jahn-Teller distortions [6,7].

II. EXPERIMENTAL METHODS

Multilayers consisting of $YBa_2Cu_3O_7$ (YBCO), $Pr_{0.5}La_{0.2}Ca_{0.3}MnO_3$ (PLCMO), and $Nd_{1-x}(Ca_{1-y}Sr_y)_xMnO_3$ (NCSMO) were grown with pulsed laser deposition (PLD) on single crystalline $La_{0.3}Sr_{0.7}Al_{0.65}Ta_{0.35}O_3$ (LSAT) substrates that are (001)-oriented (from Crystec). In the following, the sequence of the layer stacking and the individual layer thicknesses are denoted according to the growth direction and in units of nanometer, respectively. The growth was performed with an excimer KrF laser ($\lambda = 248$ nm, ts = 25 ns) with a spot size on the target of about 3 mm^2. The laser fluence was set to 1.4 J/cm^2 and the repetition rate to 2 Hz. The targets were made from densely pressed and sintered polycrystalline pellets of the corresponding materials (1-in.-diam disks with a thickness of about 5 mm) and were mounted on a rotation stage with a remote control to change between the different materials. The LSAT substrates were glued with silver paint on a stainless-steel sample holder. The backside of this holder was heated with a solid-state infrared laser, and its temperature was monitored and controlled with an internal pyrometer.

The LSAT substrate was placed about 5 cm above the targets and was heated at a rate of 20 °C min^{-1} to the deposition temperature of 825 °C at an oxygen partial pressure of 35 mbar. It was kept for at least 60 min at this temperature before the deposition was started. After the growth, the chamber was vented with pure oxygen and the sample was cooled at a rate of 10 °C min^{-1} to 480 °C. At this temperature, it was annealed for 1 h to fully oxygenate the YBCO layers. Finally, the sample was cooled to room temperature and removed from the PLD chamber and the stainless-steel sample holder. The remaining silver paint on the backside of the LSAT substrate was carefully removed.

The growth of the multilayers was monitored by *in situ* reflection high-energy electron diffraction (RHEED). For several samples, we performed *ex situ* studies with x-ray diffraction (XRD), x-ray reflectivity (XRR), polarized neutron reflectivity (PNR) and scanning transmission electron microscopy (STEM), and electron energy-loss spectrometry (EELS). Representative results can be found in the Supplemental Materials of Refs. [36,47].

Magnetotransport and dc magnetization measurements were performed with a commercial physical properties measurement system by Quantum Design (QD-PPMS) equipped with a 9 T superconducting magnet and a vibrating sample magnetometer (VSM). The resistance was measured with a four-point technique. Copper wires were glued with silver paste on the corners of the samples and a dc current of typically $I = 10$ μA was applied while the voltage was measured with a Keithley 2602 digital multimeter at a temperature ramp rate of 2 K min^{-1}. It was corrected for a small, temperature- and field-independent offset.

For the dc magnetization measurements, we used the vibrating sample magnetometer (VSM) option of the PPMS. The sample was glued (with GE Varnish) to a quartz rod and moved at a frequency of 40 Hz and peak amplitude of 2 mm. The magnetic field was applied parallel to the film plane. The data were corrected for the diamagnetic signal of the LSAT substrate that was measured at 300 K in large magnetic fields. The ferromagnetic signal of the sample arises from the manganite layers and is presented in units of μ_B/Mn using the following expression:

$$m\,[\mu_B/\mathrm{Mn}] = \frac{m\,[\mathrm{emu}]}{\mu_B\,[\mathrm{J\,T^{-1}}]} \times 10^{-3}\left[\frac{\mathrm{J}}{\mathrm{T^{-1}\,emu^{-1}}}\right] \times \frac{\text{Vol. manganite u.c.}}{\text{Vol. manganite layers}}.$$

The Raman spectra were recorded with a Jobin-Yvon LabRam HR800 spectrometer using the 632.8 nm excitation line of a HeNe laser. The measurements were carried out in full back scattering with $z(Y'X')\underline{z}$ geometry in Porto's notation. The laser was focused with a ×100 long working distance objective lens with a short depth of focus, which was positioned with an accuracy of <0.5 μm, such that the focus was in the film [48]. To further optimize the multilayer signal, a 50-μm confocal hole along the scattered light path helped to reject the signal from the LSAT substrate. The residual, weaker substrate contribution was then subtracted from the spectra using reference measurements for which the beam focus was in the substrate. Laser heating effects were minimized by keeping the laser power well below 1 mW, which resulted in a temperature uncertainty of less than 5 K [48].

III. RESULTS AND DISCUSSION

A. Recall of the insulator-superconductor transition (IST)

Figure 1(a) recalls the *R-T* curves in zero magnetic field (blue line) and at 9 T (red line) of a PLCMO(20 nm)/YBCO(7 nm)/PLCMO(20 nm) (PYP) trilayer from Ref. [36]. These were interpreted in terms of a transition from a granular superconducting state with a Coulomb blockade at zero field to a macroscopically coherent superconducting one with $T_c \approx 75$ K at 9 T.

For comparison, Fig. 1(b) shows the corresponding *R-T* curves of a single YBCO layer that has also a thickness of $d_{\mathrm{YBCO}} = 7$ nm and was grown under the same conditions as the trilayer in Fig. 1(a). The film exhibits a regular superconducting transition with $T_c \approx 80$ K already in zero magnetic field. Notably, in the normal state (above about 100 K) the zero field *R-T* curve of the trilayer in Fig. 1(a) is similar to the one of the single YBCO layer in Fig. 1(b) and they are both characteristic of a metallic response. Pronounced differences occur only below about 100 K where the trilayer shows a steep increase of the resistance that contrasts with the superconducting transition of the single YBCO layer. This shows that the highly resistive low-temperature response of the trilayer does not arise from a poor structural or chemical quality of the YBCO layer, which would also deteriorate the normal-state transport properties. Previous x-ray and HRTEM data have indeed confirmed that the YBCO layer is epitaxial and flat with atomically sharp YBCO/PLCMO interfaces and could not detect any sign of intergrowth or chemical diffusion (see the supporting online material of Ref. [36]). The *R-T* data of the trilayer are instead characteristic of a granular superconducting state of the YBCO layer that is induced via a proximity effect with the PLCMO layers. The short-ranged nature of this proximity effect with a critical length scale $d_{\mathrm{crit}} \approx 4$–5 nm (at each interface) as reported in Ref. [36] is confirmed by the *R-T* curves of a PLCMO(20 nm)/YBCO(20 nm)/PLCMO(20 nm) trilayer in Fig. 1(c), which exhibits an ordinary superconducting transition already in zero magnetic field.

The origin of this unusual proximity effect between the superconducting YBCO and the insulating manganite layers with AF and CE-type CO/OO orders remains to be understood. In the following, we explore how it depends on the electronic and magnetic properties of the manganite. Here we assume Ohmic behavior and thus neglect that the electric response in the granular superconducting state can be nonlinear, hysteretic, and characteristic of a glassy behavior as described in Ref. [36]. The discussion of these non-Ohmic effects will be the subject of a forthcoming publication.

B. Tolerance factor and IST at $x = 0.35$

At first, we discuss how the strength of the CE-type Mn-CO/OO and the underlying cooperative Jahn-Teller distortions affect the proximity effect. For this we studied a series of $Nd_{0.65}(Ca_{1-y}Sr_y)_{0.35}MnO_3$(20 nm)/YBCO(7 m)/$Nd_{0.65}(Ca_{1-y}Sr_y)_{0.35}MnO_3$(10 nm) (NYN) trilayers on LSAT with $0.2 \leqslant y \leqslant 0.5$ and corresponding tolerance factors of $0.9529 \leqslant t \leqslant 0.9565$.

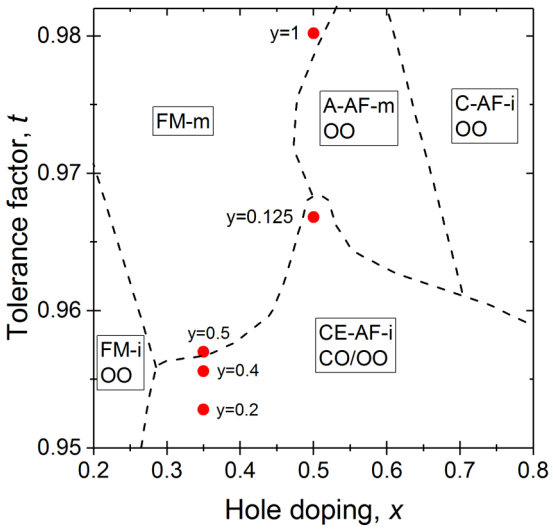

FIG. 2. Phase diagram of the different magnetic and electronic orders of manganite as a function of hole doping, x, and tolerance factor, t, sketched according to the results on single crystals reported in Refs. [7,49]. The abbreviations FM-i, FM-m, CE-AF-i, A-AF-m, and C-AF-i denote ferromagnetic-insulating, ferromagnetic-metallic, CE-type-antiferromagnetic-insulating, A-type antiferromagnetic-metallic, and C-type antiferromagnetic-insulating states, respectively. OO and CO/OO indicate orbital ordered and combined charge/orbital ordered states, respectively. Red dots show how the $Nd_{1-x}(Ca_{1-y}Sr_y)_xMnO_3$ (NCSMO) samples are located in this phase diagram.

Figure 2 shows a sketch of the expected location of these samples in the manganite phase diagram of the hole doping, x, and tolerance factor, t, according to the reported trend for corresponding bulk materials [7,49]. We assume that the NCSMO thin films have similar electronic and magnetic properties to those of their bulk counterparts. They are fairly well lattice-matched with the LSAT substrate, i.e., the pseudocubic lattice parameters of $a(\mathrm{LSAT}) = 0.387$ nm and $a(\mathrm{NCSMO}) = 0.383$–$0.384$ nm yield only a moderate tensile strain of $\Delta a/a \leqslant +1\%$. Moreover, we verified for a corresponding PLCMO(20 nm)/YBCO(7 nm)/PLCMO(20 nm) trilayer grown on a $SrLaAlO_4$ (SLAO) substrate with $a(\mathrm{SLAO}) = 0.375$ nm and $a(\mathrm{PLCMO}) = 0.386$ nm, and thus with a large compressive strain of $\Delta a/a \approx -2.8\%$, that it exhibits a similar magnetic-field-induced IST [see Fig. S1(a) in Ref. [50]] to the PYP trilayer on LSAT [see Fig. 1(a)] with only a weak compressive strain of $\Delta a/a \approx 0.3\%$. The x-ray reciprocal space maps of the PYP trilayer on SLAO suggest indeed that the strain relaxation occurs rather rapidly within the bottom PLCMO layer next to the SLAO substrate [see Fig. S1(b) in Ref. [50]] such that only weak strain effects are expected in the vicinity of the PLCMO/YBCO interface. Furthermore, we show in the following that the magnetoresistance data of the NCSMO single layers on LSAT substrates as well as the Jahn-Teller distortions seen in the Raman spectroscopy data of the corresponding trilayers agree fairly well with the phase diagram of Fig. 2.

Accordingly, for the sample with $y = 0.2$ and the smallest tolerance factor of $t = 0.9529$, we expect that the Mn-CO/OO is most pronounced and least affected by a magnetic field.

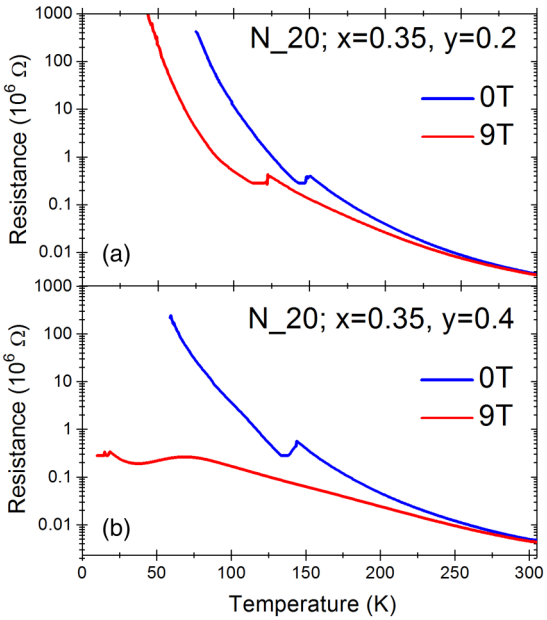

FIG. 3. Magnetoresistance vs temperature curves of $Nd_{1-x}(Ca_{1-y}Sr_y)_xMnO_3$ single layers with $x = 0.35$ and (a) $y = 0.2$ and (b) $y = 0.4$.

At $y = 0.4$ and $t = 0.9553$, the Mn-CO/OO should already be considerably weaker and more strongly suppressed by a magnetic field of the order of 9 T (our maximal field). Finally, for the sample with $y = 0.5$ and $t = 0.9565$, an itinerant FM state should be realized already at much lower fields, possibly even at zero magnetic field.

The *R-T* curves of the NSCMO(20 nm) single layers in Fig. 3 confirm the expected trend. The zero-field curve at $y = 0.2$ in Fig. 3(a) undergoes a steep, insulator-like upturn toward low temperature that is only moderately reduced at 9 T. These *R-T* curves exhibit clear anomalies around 150 K close to the AF transition but hardly any around the expected onset of the charge/orbital ordering at $T_{CO/OO} \approx 220$–240 K, at which a clear anomaly occurs in corresponding single crystals [6,7]. This is likely due to a broadening of the transition and an enhanced localization of the charge carrier at $T > T_{CO/OO}$ due to the disorder and residual strain effects that are inherent to thin films and most likely prevent the observation of a clear effect on a macroscopic scale experiment such as resistivity measurements. In fact, the development of the Mn-CO/OO below $T_{CO/OO} \approx 240$ K has been observed by micro-Raman spectroscopy in the NCSMO layer with $y = 0.2$ in terms of an anomalous temperature dependence of certain modes that are very sensitive to local Jahn-Teller distortions [47] (see also Sec. III E). The *R-T* curves of the NCSMO single layer with $y = 0.4$ in Fig. 3(b) show already a more marked magnetic field dependence. Whereas the zero-field curve still diverges toward low temperature, the resistive upturn is strongly suppressed at 9 T and saturates at low temperature toward a value that is orders of magnitude lower than at zero field (where it cannot be accurately measured anymore).

Figure 4 displays the *R-T* curves in zero magnetic field and at 9 T for the series of NSCMO(20 nm)/YBCO(7/nm)/NCSMO(10 nm) trilayers with $0.2 \leqslant y \leqslant 0.5$. Figure 4(a) shows that the $y = 0.2$ trilayer with the strongest Mn-CO/OO also exhibits the highest low temperature value of the resistance in zero magnetic field. For this sample, the 9 T magnetic field is not yet sufficient to recover a superconducting transition, i.e., the low-temperature resistance still increases below about 100 K. For the $y = 0.4$ trilayer in Fig. 4(b), the low-temperature resistance in zero magnetic field has already a considerably lower value than at $y = 0.2$, and a magnetic field of 9 T restores a regular superconducting transition. Notably, the resistive upturn of the zero-field *R-T* curve sets in only around 60 K, i.e., slightly below the onset of the superconducting transition at $T_c \approx 75$ K. Such a sharp change from a superconducting toward an insulator-like response has also been observed in conventional granular thin film superconductors (see Fig. 13 of Ref. [51]), where the grain boundaries are artificially created and the insulator transition is obtained by reducing the layer thickness. The sharp change occurs on the verge of the IST as the Coulomb-blocking starts to overcome the Josephson coupling [39,40]. For the present cuprate/manganite multilayers, the superconducting layer has no obvious granularity

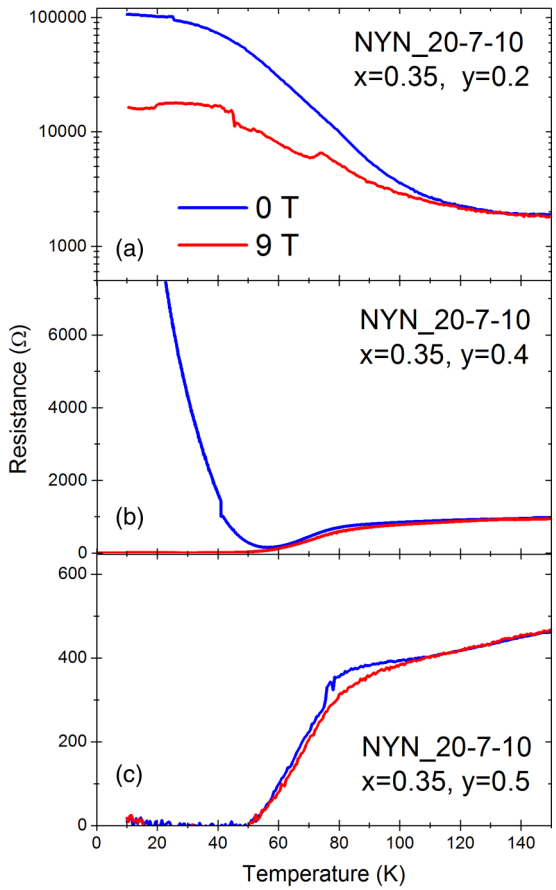

FIG. 4. Magnetoresistance vs temperature curves of NCSMO(20 nm)/YBCO(7 nm)/NCSMO(10 nm) trilayers with $x = 0.35$ and different values of y. (a) At $y = 0.2$ with a strong Mn-CO/OO that is only weakly affected by the magnetic field, (b) at $y = 0.4$ with a weaker Mn-CO/OO that is strongly suppressed at 9 T, and (c) at $y = 0.5$ where the Mn-CO/OO is very weak (or absent) already in zero magnetic field. The curves at 9 T have been normalized to the zero-field curves at high temperature.

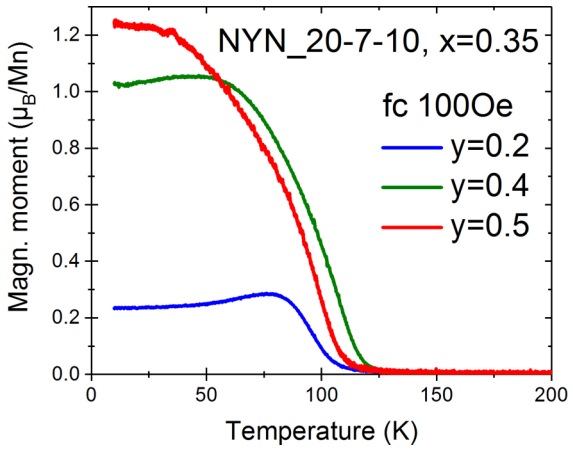

FIG. 5. Magnetization vs temperature curves of the series of NCSMO(20 nm)/YBCO(7 nm)/NCSMO(10 nm) trilayers with $x = 0.35$ with different Sr-content, y, obtained during field-cooling (fc) in 100 Oe applied parallel to the film plane. It shows that the ferromagnetic moment grows continuously as y increases and the Mn-CO/OO becomes weaker.

and its thickness is not varied to induce the superconductor-to-insulator transition. Here the Coulomb blocking seems to arise from the coupling with the neighboring manganite layers and is thus controlled by their electronic properties. Finally, for the $y = 0.5$ trilayer in Fig. 4(c), the *R-T* curve exhibits a regular superconducting transition already in zero magnetic field. The 9 T field has hardly any influence here, except for a slight broadening of the superconducting transition. The data in Fig. 4 thus establish a clear correlation between the strength of the insulator-like upturn of the *R-T* curves of these trilayers and the tolerance factor, t (as controlled by the Sr content, y), and the related strength of the Mn-CO/OO of the manganite.

C. Ferromagnetic component versus tolerance factor and hole doping

The magnetization data in Fig. 5 show that the ferromagnetic moment of the Mn ions of the above-described NYN trilayers on LSAT with $x = 0.35$ gets larger as the Sr content and thus the tolerance factor increase. For samples with a hole doping in the range $0.3 \leqslant x < 0.5$ that have an excess of Mn^{3+} ions as compared to the ideal Mn-CO/OO at $x = 0.5$ with a ratio of $Mn^{3+}/Mn^{4+} = 1$, it is well known that a ferromagnetic component coexists with the AF one [6,7,52–55]. This ferromagnetic order is associated with an insulating state and thus is distinct from the itinerant ferromagnetic state characteristic of samples with a larger tolerance factor for which the double-exchange interaction dominates [6,7]. This coexistence has been explained in terms of two different scenarios: (i) a canted AF state due to a uniaxial ferromagnetic exchange interaction of the excess Mn^{3+} ions [6,7,53,54]; and (ii) a phase-segregated state with domains of Mn-CO/OO and AF order that are spatially separated by ferromagnetic and/or disordered regions with a glassy magnetic state due to competing AF and ferromagnetic superexchange interactions [38,52]. Both scenarios are consistent with the trend displayed in Fig. 5 that shows a growing ferromagnetic moment as the tolerance factor increases and the strength of the Mn-CO/OO and the AF exchange is reduced. Irrespective of its origin, this finding suggests that the ferromagnetic order itself is not causing the proximity effect that leads to the granular superconducting state in the adjacent YBCO layers. However, it may still be playing an indirect role, for example, since the magnetic frustration that results from its competition with the antiferromagnetic interaction enhances the disorder and reduces the domain size of the Mn-CO/OO.

D. IST at $x = 0.5$

This raises the question of whether the direct coupling to the Mn-CO/OO and AF ordered state or rather an indirect one via the domain boundaries and/or the disordered regions with a frustrated and glassy charge and magnetic state is at the heart of the unusual proximity effect between YBCO and manganite. This issue has been addressed by studying samples with a hole doping of $x = 0.5$ and a nominal 1:1 ratio of Mn^{3+}/Mn^{4+}, i.e., free of excess Mn^{3+} ions that disrupt the long-range Mn-CO/OO and AF order [6,7,38,55].

Figure 6 displays the magnetization and the *R-T* curves of a single NCSMO(20 nm) layer on LSAT with $x = 0.5$, $y = 0.125$, and $t = 0.9668$. The low-field magnetization curves in Fig. 6(a) at 10 and 100 mT show a very small magnetic moment of less than $0.1\,\mu_B$/Mn, as expected for a sample with a long-range Mn-CO/OO and AF order without significant spin canting or phase segregation. The high-field *M-H* loops in Fig. 6(b) also exhibit only a gradual enhancement of the magnetic moment to about $1.2\,\mu_B$/Mn − ion at 9 T and 5 K. The corresponding *R-T* curves in Fig. 6(c) reveal a steep resistive upturn in zero field that is hardly reduced at 9 T suggesting that the Mn-CO/OO remains very strong at 9 T. This agrees with the reported trend of $Pr_{0.5}Ca_{0.5}MnO_3$ single crystals with a comparable tolerance factor $t = 0.9659$, for which a magnetic field larger than 20 T is required to suppress the Mn-CO/OO [6,7].

The *R-T* curves of the corresponding trilayer on LSAT with $x = 0.5$ and $y = 0.125$ are displayed in Fig. 7. Notably, they reveal the same type of magnetic-field-induced transition from a low-field state with an insulator-like low-temperature response to a high-field state with a regular superconducting transition. However, despite the very strong Mn-CO/OO, the low-temperature value of the resistance is considerably lower than for the trilayer at $x = 0.35$ and $y = 0.2$. Moreover, the sudden increase of the resistance sets in around 60 K well below the onset of the superconducting transition at $T_c \approx 75$ K. The overall trend resembles the one of the trilayer with $x = 0.35$ and $y = 0.4$ for which the Mn-CO/OO is rather weak and strongly affected by the 9 T magnetic field, as confirmed by the *R-T* curves of the corresponding NCSMO single layer in Fig. 3(b). This suggests that the proximity effect underlying the IST probably does not involve a direct coupling to the Mn-CO/OO, which is considerably stronger at $x = 0.5$ and $y = 0.125$ than at $x = 0.35$ and $y = 0.4$ (see also the Raman data in Sec. III E). It rather seems that the domain boundaries of the Mn-CO/OO and the disordered regions due to the excess Mn^{3+} ions, which are more abundant for $x = 0.35$ than $x = 0.5$, are playing an important role in this proximity effect.

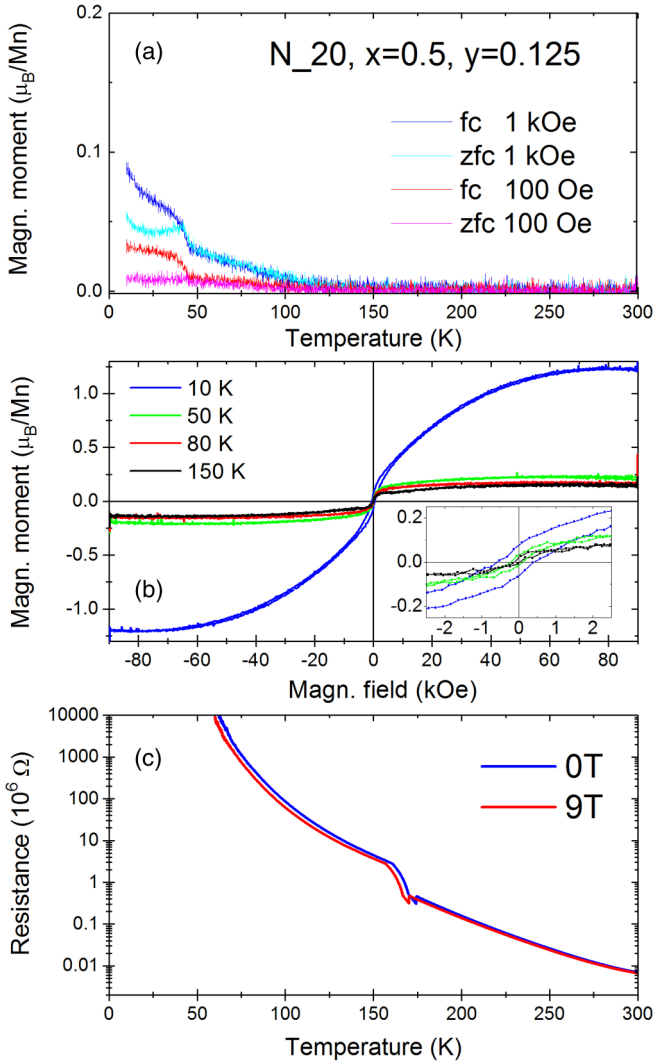

FIG. 6. Magnetic and magnetoelectric properties of a single NCSMO(20 nm) layer with $x = 0.5$ and $y = 0.125$. (a) Low-field magnetization data in field-cooling (fc) and zero-field-cooling (zfc) mode, which confirm the absence of a sizeable ferromagnetic moment. (b) Magnetization vs field (M-H) loops, which reveal that a weak ferromagnetic moment is induced by a high field only at low temperature (below 50 K). (c) R-T curves showing a very steep resistive upturn that is hardly affected by a field of 9 T.

Finally, Fig. 8 displays the R-T curves of single-layer and corresponding trilayer samples on LSAT with $x = 0.5$, $y = 1$, and $t = 0.9837$, i.e., NSMO, where all Ca atoms were substituted by Sr. The R-T curves of the single layer in Fig. 8(a) reveal a metallic low-temperature response with a pronounced maximum around the Curie-temperature $T_{\text{Curie}} \approx 230$ K in zero magnetic field that is suppressed and shifted to higher temperature by a magnetic field. The overall behavior is characteristic of an itinerant ferromagnetic state based on the double-exchange interaction, as it is commonly observed in samples with a sufficiently large tolerance factor, such as in $La_{1-x}(Ca, Sr)_xMnO$ with $0.25 < x < 0.5$ [6,7]. The R-T curves of the corresponding trilayer in Fig. 8(b) show indeed no sign of a resistive upturn due to a granular superconducting state. A regular superconducting

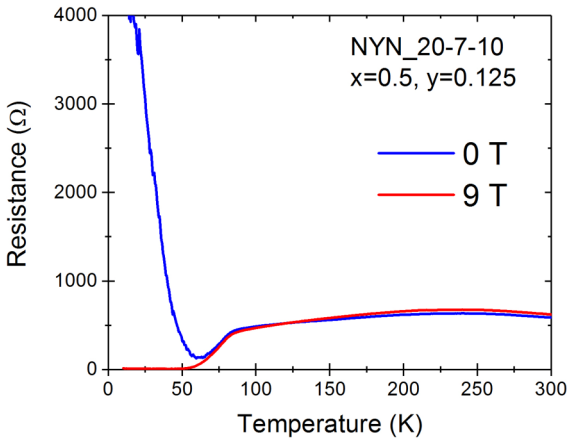

FIG. 7. R-T curves of the NCSMO(20 nm)/YBCO(7 nm)/NCSMO(10 nm) trilayer with $x = 0.5$ and $y = 0.125$, which exhibits a magnetic-field-induced transition from a low-field state with an insulator-like low-temperature response to a high-field state with a regular superconducting transition.

transition occurs here already in zero magnetic field, and the largest magnetoresistance effect occurs in the normal state, in particular around the Curie temperature $T_{\text{Curie}} \approx 225$ K that is indicated by the broad maximum in the R-T curve in zero

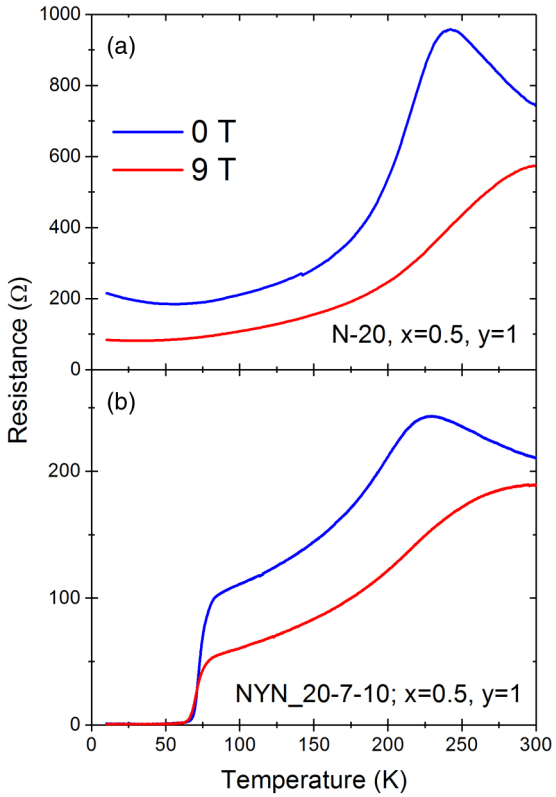

FIG. 8. Magnetoresistance vs temperature curves of (a) a NCSMO(20 nm) single layer with $x = 0.5$ and $y = 1$, and (b) a corresponding NCSMO(20 nm)/YBCO(7 nm)/NCSMO(10 nm) trilayer with $x = 0.5$ and $y = 1$. The trilayer exhibits a regular superconducting transition already in zero magnetic field, and the major magnetic field effect occurs in the normal state due to the magnetoresistance of the NCSMO layer.

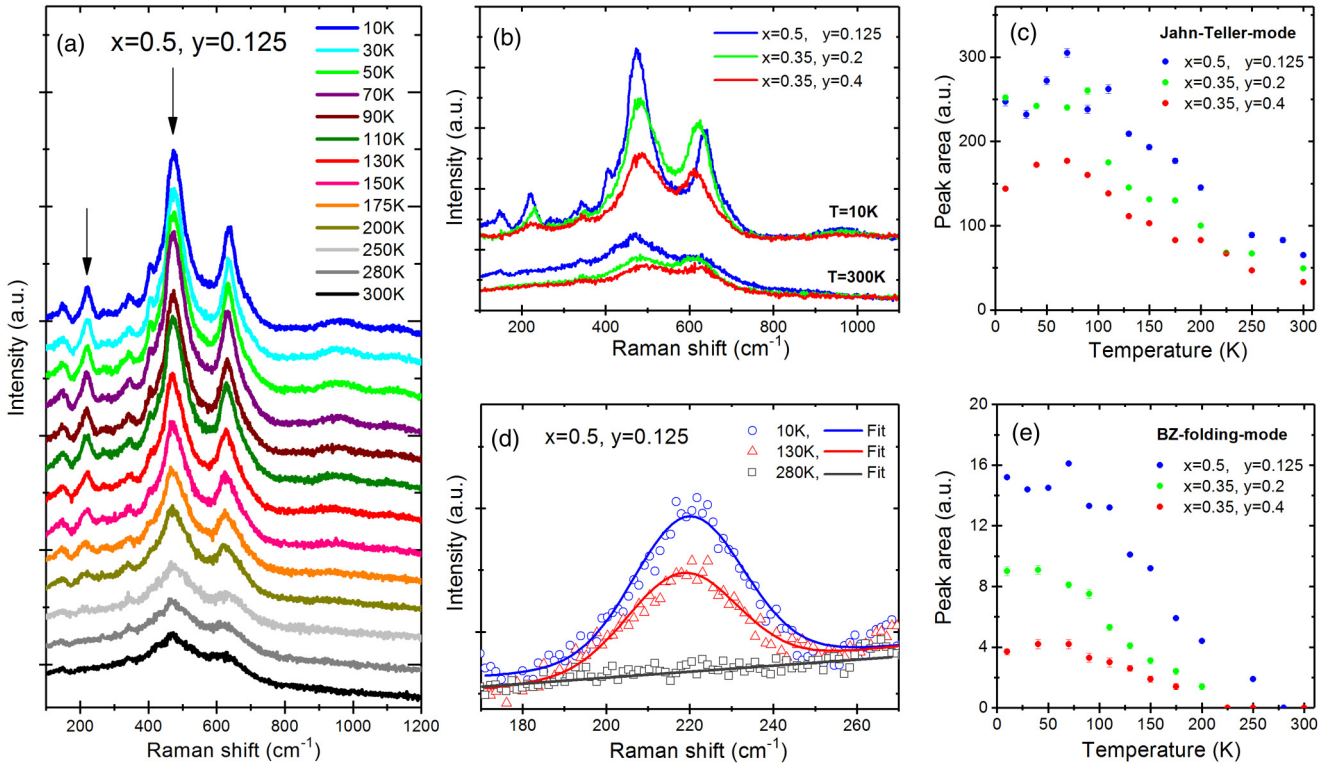

FIG. 9. (a) Temperature-dependent Raman-spectra of the NCSMO(20 nm)/YBCO(7 nm)/NCSMO(10 nm) trilayer with $x = 0.5$ and $y = 0.125$. Vertical offsets are added for clarity. The arrows mark the position of the "Jahn-Teller-mode" around 480 cm^{-1} and a weaker mode around 225 cm^{-1} that arises from the folding of the Brillouin-zone ("BZ-folding mode") and thus appears only in the Mn-CO/OO state. (b) Comparison of the Raman spectra at 300 and 10 K for the trilayers with $x = 0.5$ and 0.35. For the 10 K spectra, a vertical offset has been added for clarity. (c) Temperature dependence of the intensity of the Jahn-Teller mode obtained by fitting with Gaussian profiles. (d) Magnified view of the BZ-folding mode and Gaussian fits at selected temperatures. (e) Comparison of the temperature dependence of the intensity of the BZ-folding mode for the $x = 0.5$ and 0.35 trilayers. The error bars in (c) and (e) represent the accuracy of the fitting procedure.

magnetic field. Note that in this case there is a significant conduction channel through both the YBCO and manganite layer due to their comparable resistivity values, whereas for the trilayers with insulating manganites conduction is dominantly through the YBCO layer.

E. Mn-CO/OO probed with Raman spectroscopy

Measurements on single crystals have shown that some Raman modes of the manganites are very sensitive to the onset of the Mn-CO/OO [56]. These modes are symmetry-forbidden for the undistorted cubic perovskite structure, and their intensity is proportional to the magnitude of the Jahn-Teller-type lattice distortions that accompany the Mn-CO/OO state. Examples are the so-called "Jahn-Teller mode" around 480 cm^{-1} and the "breathing mode" around 620 cm^{-1}, both of which exhibit an anomalous temperature dependence due to the enhancement of the Jahn-Teller-type distortions in the Mn-CO/OO state. Their nonzero intensity above the Mn-CO/OO transition can be understood in terms of an order-disorder transition with a high-temperature state of strongly disordered and fluctuating Jahn-Teller distortions [56]. These anomalous Raman modes have already been studied for the NYN trilayers with $x = 0.35$ for which it was shown that the Mn-CO/OO is considerably stronger at $y = 0.2$ than at $y = 0.4$ [45].

Figure 9 shows the corresponding Raman data of the trilayer with $x = 0.5$ and $y = 0.125$ in comparison to the trilayers with $x = 0.35$. Figure 9(a) displays the temperature-dependent Raman spectra of the trilayer with $x = 0.5$. A comparison between the Raman spectra of the NYN trilayers with $x = 0.5$ and 0.35 is shown in Fig. 9(b) for measurements at 300 and 10 K. It reveals that at 10 K the Raman modes related to the Mn-CO/OO are more pronounced and sharper for the $x = 0.5$ trilayer than at $x = 0.35$. This trend is confirmed by the temperature evolution of the intensity of the Jahn-Teller mode around 480 cm^{-1} of the three NYN trilayers, as obtained from fits with Gaussian profiles, displayed in Fig. 9(c). The stronger and more long-ranged nature of the Mn-CO/OO at $x = 0.5$, as compared to the one at $x = 0.35$, is also evident from the comparison of the weaker phonon mode around 225–230 cm^{-1}, shown in Figs. 9(d) and 9(e). This mode appears only in the Mn-CO/OO state and arises most likely from the folding of the Brillouin zone due to the enlarged unit cell in the Mn-CO/OO state [56]. Its intensity, which thus is a good measure of the magnitude of the lattice distortions that accompany the Mn-CO/OO, is also considerably larger for $x = 0.5$ than for $x = 0.35$. The Raman data thus highlight that the Mn-CO/OO of the trilayer with $x = 0.5$ and $y = 0.125$ is stronger and, likely, more long-ranged than that of the corresponding trilayers with $x = 0.35$ and $y = 0.2$ or 0.4.

IV. SUMMARY AND CONCLUSION

We have found that the insulator-like low-temperature response of the manganite/YBCO/manganite trilayers, which involves a granular superconducting state of the YBCO layer with a strong Coulomb blocking that overcomes the Josephson coupling between the grains [36], occurs only in the presence of a CE-type AF and Mn-CO/OO order of the manganite layers. In particular, for trilayers with a manganite hole doping of $x = 0.35$, we have shown that this proximity effect vanishes as the Mn-CO/OO gets suppressed either with a large magnetic field or by increasing the tolerance factor of the manganite. Nevertheless, we obtained evidence that this intriguing proximity effect does not directly involve the long-range Mn-CO/OO but rather the related domain boundaries and/or the disordered regions with a glassy charge and magnetic state. The localization of the superconducting charge carriers, due to a Coulomb blocking that overcomes the Josephson coupling between the superconducting grains, is indeed much weaker for a trilayer with $x = 0.5$ and $y = 0.125$, and a long-ranged Mn-CO/OO, than for a trilayer with $x = 0.35$ and $y = 0.2$, for which the Mn-CO/OO is more disordered.

The microscopic mechanism underlying the formation of the granular superconducting state in the YBCO layer, i.e., whether it involves the spin, charge, or orbital channel (or a combination of them), remains an open issue. It may even be based on the Jahn-Teller-type lattice distortions that accompany the Mn-CO/OO since a strong coupling between the phonons of the cuprate and manganite layers was previously reported [57]. Moreover, it remains to be clarified whether the disorder and the domain boundaries of the Mn-CO/OO are directly "imprinted" as superconducting grain boundaries into the YBCO layer. Alternatively, they may stabilize a charge- or spin-ordered state in the YBCO layer [32,47] that forms its own domain state and competes with superconductivity or possibly even gives rise to an intertwined state with domain boundaries at which the superconducting coherence is broken [58].

Despite all of these open questions, an appealing aspect of this kind of superconducting proximity effect is that it can be controlled and tuned via external parameters, like a magnetic field, applied current, and likely even photons. These manganite/cuprate multilayers thus can serve as a platform to study and manipulate the interaction of high-T_c superconductivity with its various competing charge, orbital, and/or spin orders. The phase diagram of the manganites also provides us with several additional spin, charge, and orbital ordered states [6,7] for which it remains to be explored how they affect the superconducting state of adjacent cuprate layers.

ACKNOWLEDGMENTS

The work at the University of Fribourg was supported by the Swiss National Foundation (SNSF) through Grants No. 200020-172611 and CRSII2-154410/1. B.P.P.M. acknowledges support from the Rutherford Foundation of New Zealand, and B.K. and M.M acknowledge the funding from the Deutsche Forschungsgemeinschaft (DFG, German Research Foundation)–Projektnummer 107745057–TRR 80.

[1] J. G. Bednorz and K. A. Müller, Z. Phys. B **64**, 189 (1986).
[2] R. von Helmolt, J. Wecker, B. Holzapfel, L. Schultz, and K. Samwer, Phys. Rev. Lett. **71**, 2331 (1993).
[3] M. Imada, A. Fujimori, and Y. Tokura, Rev. Mod. Phys. **70**, 1039, (1998).
[4] H. Y. Hwang, Y. Iwasa, M. Kawasaki, B. Keimer, N. Nagaosa, and Y. Tokura, Nat. Mater. **11**, 103 (2012).
[5] E. Dagotto, Science **318**, 1076 (2007).
[6] Y. Tokura and Y. Tomioka, J. Magn. Magn. Mater. **200**, 1 (1999).
[7] J. Tokura, Rep. Prog. Phys. **69**, 797 (2006).
[8] B. Keimer, S. A. Kivelson, M. R. Norman, S. Uchida, and J. Zaanen, Nature (London) **518**, 179 (2015).
[9] J. M. Tranquada, J. D. Axe, N. Ichikawa, A. R. Moodenbaugh, Y. Nakamura, and S. Uchida, Phys. Rev. Lett. **78**, 338 (1997).
[10] G. Ghiringhelli, M. Le Tacon, M. Minola, S. Blanco-Canosa, C. Mazzoli, N. B. Brookes, G. M. De Luca, A. Frano, D. G. Hawthorn, F. He, T. Loew, M. Moretti Sala, D. C. Peets, M. Salluzzo, E. Schierle, R. Sutarto, G. A. Sawatzky, E. Weschke, B. Keimer, and L. Braicovich, Science **337**, 821 (2012); J. Chang, E. Blackburn, A. T. Holmes, N. B. Christensen, J. Larsen, J. Mesot, R. Liang, D. A. Bonn, W. N. Hardy, A. Watenphul, M. V. Zimmermann, E. M. Forgan, and S. M. Hayden, Nat. Phys. **8**, 871 (2012); A. J. Achkar, R. Sutarto, X. Mao, F. He, A. Frano, S. Blanco-Canosa, M. Le Tacon, G. Ghiringhelli, L. Braicovich, M. Minola, M. Moretti Sala, C. Mazzoli, R. Liang, D. A. Bonn, W. N. Hardy, B. Keimer, G. A. Sawatzky, and D. G. Hawthorn, Phys. Rev. Lett. **109**, 167001 (2012); R. Comin, A. Frano, M. M. Yee, Y. Yoshida, H. Eisaki, E. Schierle, E. Weschke, R. Sutarto, F. He, A. Soumyanarayanan, Y. He, M. Le Tacon, I. S. Elfimov, J. E. Hoffman, G. A. Sawatzky, B. Keimer, and A. Damascelli, Science **343**, 390 (2014); M. Hashimoto, G. Ghiringhelli, W.-S. Lee, G. Dellea, A. Amorese, C. Mazzoli, K. Kummer, N. B. Brookes, B. Moritz, Y. Yoshida, H. Eisaki, Z. Hussain, T. P. Devereaux, Z.-X. Shen, and L. Braicovich, Phys. Rev. B **89**, 220511(R) (2014); E. H. da Silva Neto, R. Comin, F. He, R. Sutarto, Y. Jiang, R. L. Greene, G. A. Sawatzky, and A. Damascelli, Science **347**, 282 (2015); E. H. da Silva Neto, B. Yu, M. Minola, R. Sutarto, E. Schierle, F. Boschini, M. Zonno, M. Bluschke, J. Higgins, Y. Li, G. Yu, E. Weschke, F. He, M. Le Tacon, R. L. Greene, M. Greven, G. A. Sawatzky, B. Keimer, and A. Damascelli, Sci. Adv. **2**, e1600782 (2016).
[11] H. M. Christen and G. Eres, J. Phys.: Condens. Matter **20**, 264005 (2008).
[12] A. Ohtomo and H. Y. Hwang, Nature (London) **427**, 423 (2004).
[13] M. Bibes, J. E. Villegas, and A. Barthelemy, Adv. Phys. **60**, 5 (2011).
[14] P. Przyslupski, S. Kolesnik, E. Dynovska, T. Skoskiewicz, and M. Sawicki, IEEE T. Appl. Supercond. **7**, 2192 (1997).
[15] A. M. Goldman, P. I. Kraus, K. Nikolaev, V. Vas'ko, A. Bhattacharya, and W. Cooley, J. Supercond. **14**, 283 (2001).
[16] H. U. Habermeier and G. Cristiani, J. Supercond. **15**, 425 (2002).

[17] Z. Sefrioui, D. Arias, V. Peña, J. E. Villegas, M. Varela, P. Prieto, C. León, J. L. Martinez, and J. Santamaria, Phys. Rev. B **67**, 214511 (2003).

[18] M. Varela, A. R. Lupini, S. J. Pennycook, Z. Sefrioui, and J. Santamaria, Solid-State Electron. **47**, 2245 (2003).

[19] T. Holden, H.-U. Habermeier, G. Cristiani, A. Golnik, A. Boris, A. Pimenov, J. Humlíček, O. I. Lebedev, G. Van Tendeloo, B. Keimer, and C. Bernhard, Phys. Rev. B **69**, 064505 (2004).

[20] V. Peña, Z. Sefrioui, D. Arias, C. Leon, J. Santamaria, J. L. Martinez, S. G. E. te Velthuis, and A. Hoffmann, Phys. Rev. Lett. **94**, 057002 (2005).

[21] J. Stahn, J. Chakhalian, Ch. Niedermayer, J. Hoppler, T. Gutberlet, J. Voigt, F. Treubel, H.-U. Habermeier, G. Cristiani, B. Keimer, and C. Bernhard, Phys. Rev. B **71**, 140509(R) (2005).

[22] A. Hoffmann, S. G. E. te Velthuis, Z. Sefrioui, J. Santamaría, M. R. Fitzsimmons, S. Park, and M. Varela, Phys. Rev. B **72**, 140407(R) (2005).

[23] V. Peña, T. Gredig, J. Santamaria, and I. K. Schuller, Phys Rev. Lett. **97**, 177005 (2006).

[24] J. Chakhalian, J. W. Freeland, G. Srajer, J. Strempfer, G. Khaliullin, J. C. Cezar, T. Charlton, R. Dalgliesh, C. Bernhard, G. Cristiani, H.-U. Habermeier, and B. Keimer, Nat. Phys. **2**, 244 (2006).

[25] J. Chakhalian, J. W. Freeland, H. U. Habermeier, G. Cristiani, G. Khaliullin, M. van Veenendaal, and B. Keimer, Science **318**, 1114 (2007).

[26] J. Hoppler, J. Stahn, Ch. Niedermayer, V. K. Malik, H. Bouyanfif, A. J. Drew, M. Rössle, A. Buzdin, G. Cristiani, H.-U. Habermeier, B. Keimer, and C. Bernhard, Nat. Mater. **8**, 315 (2009).

[27] Y. Kalcheim, T. Kirzhner, G. Koren, and O. Millo, Phys. Rev. B **83**, 064510 (2011).

[28] V. K. Malik, I. Marozau, S. Das, B. Doggett, D. K. Satapathy, M. A. Uribe-Laverde, N. Biskup, M. Varela, C. W. Schneider, C. Marcelot, J. Stahn, and C. Bernhard, Phys. Rev. B **85**, 054514 (2012).

[29] D. K. Satapathy, M. A. Uribe-Laverde, I. Marozau, V. K. Malik, S. Das, Th. Wagner, C. Marcelot, J. Stahn, S. Brück, A. Rühm, S. Macke, T. Tietze, E. Goering, A. Frañó, J.-H. Kim, M. Wu, E. Benckiser, B. Keimer, A. Devishvili, B. P. Toperverg, M. Merz, P. Nagel, S. Schuppler, and C. Bernhard, Phys. Rev. Lett. **108**, 197201 (2012).

[30] C. Visani, Z. Sefrioui, J. Tornos, C. Leon, J. Briatico, M. Bibes, A. Barthélémy, J. Santamaría, and J. E. Villegas, Nat. Phys. **8**, 539 (2012).

[31] M. Egilmez, J. W. A. Robinson, J. L. MacManus-Driscoll1, L. Chen, H. Wang, and M. G. Blamire, Europhys. Lett. **106**, 37003 (2014).

[32] A. Frano, S. Blanco-Canosa, E. Schierle, Y. Lu, M. Wu, M. Bluschke, M. Minola, G. Christiani, H. U. Habermeier, G. Logvenov, Y. Wang, P. A. van Aken, E. Benckiser, E. Weschke, M. Le Tacon, and B. Keimer, Nat. Mater. **15**, 831 (2016).

[33] K. Sen, E. Perret, A. Alberca, M. A. Uribe-Laverde, I. Marozau, M. Yazdi-Rizi, B. P. P. Mallett, P. Marsik, C. Piamonteze, Y. Khaydukov, M. Döbeli, T. Keller, N. Biškup, M. Varela, J. Vašátko, D. Munzar, and C. Bernhard, Phys. Rev. B **93**, 205131 (2016).

[34] M. Eschrig, Phys. Today **64**, 43 (2011).

[35] J. W. A. Robinson and J. Linder, Nat. Phys. **11**, 307 (2015).

[36] B. P. P. Mallett, J. Khmaladze, P. Marsik, E. Perret, A. Cerreta, M. Orlita, N. Biškup, M. Varela, and C. Bernhard, Phys. Rev. B **94**, 180503(R) (2016).

[37] V. Ferrari, M. Towler, and P. B. Littlewood, Phys. Rev. Lett. **91**, 227202 (2003).

[38] Ch. Jooss, L. Wu, T. Beetz, R. F. Klie, M. Beleggia, M. A. Schofield, S. Schramm, J. Hoffmann, and Y. Zhu, Proc. Natl. Acad. Sci. (USA) **104**, 13597 (2007).

[39] V. F. Gantmakher and V. T. Dolgopolov, Phys. Usp. **53**, 1 (2010).

[40] A. M. Goldman, Int. J. Mod. Phys. B **24**, 4081 (2010).

[41] V. Jaccarino and M. Peter, Phys. Rev. Lett. **9**, 290 (1962).

[42] H. W. Meul, C. Rossel, M. Decroux, O. Fischer, G. Remenyi, and A. Briggs, Phys. Rev. Lett. **53**, 497 (1984).

[43] S. Uji, H. Shinagawa, T. Terashima, T. Yakabe, Y. Terai, M. Tokumoto, A. Kobayashi, H. Tanaka, and H. Kobayashi, Nature (London) **410**, 908 (2001).

[44] M. Tian, N. Kumar, S. Xu, J. Wang, J. S. Kurtz, and M. H. W. Chan, Phys. Rev. Lett. **95**, 076802 (2005).

[45] Y. Chen, S. D. Snyder, and A. M. Goldman, Phys. Rev. Lett. **103**, 127002 (2009).

[46] H. S. J. van der Zant, W. J. Elion, L. J. Geerligs, and J. E. Mooij, Phys. Rev. B **54**, 10081 (1996); R. Fazio and H. van der Zant, Phys. Rep. **355**, 235 (2001).

[47] E. Perret, C. Monney, S. Johnston, J. Khmaladze, F. Lyzwa, R. Gaina, M. Dantz, J. Pelliciari, C. Piamonteze, B. P. P. Mallett, M. Minola, B. Keimer, T. Schmitt, and C. Bernhard, Commun. Phys. **1**, 45 (2018).

[48] M. Hepting, M. Minola, A. Frano, G. Cristiani, G. Logvenov, E. Schierle, M. Wu, M. Bluschke, E. Weschke, H.-U. Habermeier, E. Benckiser, M. Le Tacon, and B. Keimer, Phys. Rev. Lett. **113**, 227206 (2014).

[49] Y. Tomioka, A. Asamitsu, H. Kuwahara, and Y. Tokura, J. Phys. Soc. Jpn. **66**, 302 (1997).

[50] See Supplemental Material at http://link.aps.org/supplemental/10.1103/PhysRevMaterials.3.084801 for additional x-ray and transport data showing the influence of strain from the substrate on the insulator-superconductor transition.

[51] I. S. Beloborodov, A. V. Lopatin, V. M. Vinokur, and K. B. Efetov, Rev. Mod. Phys. **79**, 469 (2007).

[52] Z. Jirák, S. Krupička, Z. Šimša, M. Dlouhá, and S. Vratislav, J. Magn. Magn. Mater. **53**, 153 (1985).

[53] H. Yoshizawa, H. Kawano, Y. Tomioka, and Y. Tokura, Phys. Rev. B **52**, 13145(R) (1995).

[54] R. Kajimoto, H. Mochizuki, H. Yoshizawa, S. Okamoto, and S. Ishihara, Phys. Rev. B **69**, 054433 (2004).

[55] S. Y. Zhou, Y. Zhu, M. C. Langner, Y.-D. Chuang, P. Yu, W. L. Yang, A. G. Cruz Gonzalez, N. Tahir, M. Rini, Y.-H. Chu, R. Ramesh, D.-H. Lee, Y. Tomioka, Y. Tokura, Z. Hussain, and R. W. Schoenlein, Phys Rev. Lett. **106**, 186404 (2011).

[56] V. Dediu, C. Ferdeghini, F. C. Matacotta, P. Nozar, and G. Ruani, Phys. Rev. Lett. **84**, 4489 (2000).

[57] N. Driza, S. Blanco-Canosa, M. Bakr, S. Soltan, M. Khalid, L. Mustafa, K. Kawashima, G. Christiani, H-U. Habermeier, G. Khaliullin, C. Ulrich, M. Le Tacon, and B. Keimer, Nat. Mater. **11**, 675 (2012).

[58] E. Fradkin, S. A. Kivelson, and J. M. Tranquada, Rev. Mod. Phys. **87**, 457 (2015).